Journal of Molecular Catalysis A: Chemical 335 (2011) 210–221

Contents lists available at ScienceDirect

Journal of Molecular Catalysis A: Chemical

journal homepage: www.elsevier.com/locate/molcata

Characterization of palladium oxide catalysts supported on nanoparticle metal oxides for the oxidative coupling of 4-methylpyridine

Luke M. Neal, Michael L. Everett, Gar B. Hoflund, Helena E. Hagelin-Weaver*

Department of Chemical Engineering, University of Florida, Gainesville, FL 32611, United States

ARTICLE INFO

Article history:
Received 14 July 2010
Received in revised form 1 November 2010
Accepted 26 November 2010
Available online 8 December 2010

Keywords:
Palladium
Nanoparticle oxide
4-Methylpyridine
C–H activation
Aromatic coupling

ABSTRACT

Palladium catalysts supported on various metal oxides were characterized using X-ray photoelectron spectroscopy (XPS), X-ray diffraction (XRD) and transmission electron microscopy (TEM) to investigate why these catalysts do not show any correlation between the measured Pd surface area and the catalytic activity for the oxidative coupling of 4-methylpyridine to 4,4′-dimethyl-2,2′-bipyridine.

The XPS data confirm the classification of n-Al_2O_3(+), n-MgO and p-SiO_2 as non-interacting supports, since the Pd $3d_{5/2}$ binding energy (BE) of palladium on these supports is 336.1 eV, consistent with bulk PdO. In contrast, catalysts supported on p-TiO_2, n-ZnO, n-ZrO_2, n-ZrO_2(CeO_2), and n-CeO_2 have Pd $3d_{5/2}$ BEs ranging from 336.3 to 337.4 eV, which reveal varying degrees of metal-support interactions. Metal support interactions leading to electron deficient Pd^{2+} species are likely beneficial for the reaction due to a facilitated C–H insertion step.

While both the PdO/p-TiO_2 and PdO/n-TiO_2 catalysts have a Pd 3d BE of 336.3 eV, their differences in activity can be attributed to (1) the PdO/n-TiO_2 catalyst as prepared having a significantly higher number of hydroxyl groups on the surface compared with the PdO/p-TiO_2 catalyst, and (2) the p-TiO_2 support being crystalline with an anatase phase, while the n-TiO_2 support is nearly amorphous. The presence of surface hydroxyl groups before reaction could hinder the first C–H activation step, and an anatase phase of the support can result in more favorable palladium-support interactions compared with an amorphous TiO_2. The XPS data also indicates that while Pd-support interactions are beneficial, very strong interactions, such as in the case of CeO_2, can lead to migration of the support over Pd, which reduces the Pd surface area and explains the lower than expected activity of the PdO/n-CeO_2 catalyst.

On some supports in this study leaching may occur during the reaction, but the characterization data indicate that other factors of catalyst deactivation are more important. XRD reveals that the complete reduction of the PdO particles on the surface is very fast compared to the reaction time. This observation explains why reducible supports with mobile oxygen are beneficial in this reaction. These supports can facilitate the reoxidation of palladium due to strong metal-support interactions. Migration of the support over the active palladium species is another deactivation pathway that appears to be more severe than leaching on these catalysts.

1. Introduction

Palladium is an excellent oxidation catalyst that has been used in both complete oxidation reactions of various compounds [1–8] and selective oxidation reactions, such as conversion of hexane to benzene [9] and oxidation of alcohols to aldehydes or ketones [10]. C–C coupling reactions are also commonly catalyzed by palladium complexes [11,12]. While many C–C coupling reactions involve halogenated compounds, palladium can insert into C–H bonds and bring about C–C coupling without halogenated precursors [13]. The C–H activation and C–C coupling of 4-methyl pyridine, as well as other pyridine derivatives, over palladium catalysts has been reported in the literature [14–16]. These reactions are often slow with low yields, resulting in relatively high prices for these products; such as $5640 per kg for 4,4′-dimethyl-2,2′-bipyridine [17]. However, this reaction is a relatively simple one-step process (Scheme 1) with environmental benefits as water and the terpyridine are the only byproducts and halogenated precursors are avoided. Improving these palladium/palladium oxide catalysts through a better understanding of their activity is desirable.

The most commonly used palladium catalyst for the coupling of 4-methylpyridine is palladium on carbon (Pd/C), while commercial palladium on alumina (Pd/Al_2O_3) has been reported to be inactive [14–16,18]. Recent research has demonstrated that

* Corresponding author at: Department of Chemical Engineering, University of Florida, P.O. Box 116005, Gainesville, FL 32611, United States. Tel.: +1 352 392 6585; fax: +1 352 392 9513.
E-mail address: hweaver@che.ufl.edu (H.E. Hagelin-Weaver).

1381-1169/$ – see front matter © 2010 Elsevier B.V. All rights reserved.
doi:10.1016/j.molcata.2010.11.036

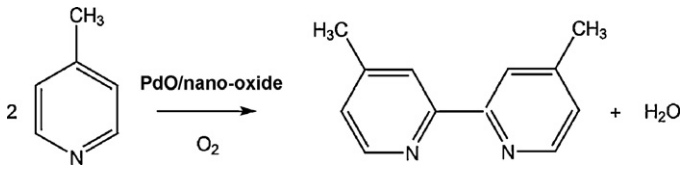

Scheme 1. Oxidative coupling of 4-methylpyridine over a palladium oxide catalyst.

alumina-supported catalysts can be active in the coupling reaction of 4-methylpyridine, but the activity is dependent on the type of alumina support and the preparation method [19]. The best catalysts to date for this reaction are 5% palladium precipitated onto alumina nanoparticles (PdO/n-Al_2O_3(+) [20]) or porous titania (PdO/p-TiO_2 [21]), with yields of 2.5–2.6 g of product per g of catalyst or 50–52 g/g palladium [19,22]. Other supports, such as nanoparticle magnesia, zirconia, ceria-doped zirconia and zinc oxide, can also be used to prepare active catalysts [22]. This represents a wide range of supports with varying properties. In previous research the measured Pd dispersion and the number of acidic or basic sites of the supports were found to have no simple correlation with activity. The most active catalysts were prepared using either high surface area supports (>400 m^2/g) or using oxides which have been shown to exhibit strong metal-support interactions with palladium [22].

A detailed investigation has been carried out in which selected catalysts were subjected to (I) X-ray photoelectron spectroscopy (XPS) to probe the surface composition and chemical states of the palladium phase in the fresh and spent catalyst, (II) transmission electron microscopy (TEM) to image the structure and palladium dispersion of prepared catalysts, and (III) X-ray diffraction (XRD) to determine the crystal structure and particle sizes of the catalyst supports. The objective of this study was to determine if the measured properties correlate with the activity of these catalysts.

2. Experimental

2.1. Catalyst preparation and reaction

A number of 5 wt% Pd catalysts supported on various oxides [22] were carefully characterized using XPS, XRD and TEM to obtain structural and compositional information. The catalysts included in this study are palladium oxide supported on: nanoparticle titania (n-TiO_2), porous titania, (p-TiO_2), nanoparticle ceria (n-CeO_2), nanoparticle zirconia (n-ZrO_2), CeO_2-doped ZrO_2 nanoparticles (10% CeO_2: n-ZrO_2(CeO_2)), nanoparticle magnesium oxide (n-MgO), nanoparticle zinc oxide (n-ZnO) and porous silica (p-SiO_2) [23]. These catalysts were prepared by precipitation of palladium nitrate onto the supports from an aqueous solution by sodium hydroxide as described in previous work [19]. More specifically, 1.9 g of support was dispersed in 100 ml of water under constant stirring. $Pd(NO_3)_2$ (0.25 g) was dissolved in 5 ml deionized H_2O and was poured into the support/water mixture. $Pd(OH)_2$ was deposited onto the support by adding, dropwise, 100 ml of a NaOH solution containing a 50% stoichiometric excess of base (0.028 M) to the resulting dispersion under vigorous stirring at room temperature. The precipitate was then aged over night before it was filtered, redispersed in deionized water and left under continuous stirring for another 20 h. The aging step was necessary to prepare a reproducible and active catalyst and washing was necessary to remove residual sodium ions and any chloride contaminant as these can accumulate on the surface and reduce activity. Washing the catalyst by redispersing in water and stirring over night is the most efficient procedure to remove the contaminants as these catalysts are difficult to filter. The same preparation method was used for all catalysts under investigation. Only for supports that form very dense aggregates, such as the nanoparticle alumina minus [26], did this preparation method result in palladium deposition only on the outermost surface of the support. The reaction data from these catalysts has been presented previously and the results are summarized in Table 1. The catalysts were used in the reactions without reduction.

After exposure to the reaction conditions (reflux in 4-methylpyridine for 72 h), the spent catalysts were recovered using a glass micro-fiber filter and washed with chloroform three times to remove the product. After filtration, they were dried briefly at room temperature before they were placed in the XPS system.

Reduced catalysts were prepared by reduction in 5% hydrogen in nitrogen for 1 h at 170 °C, outgassed in nitrogen at 170 °C for an additional hour and then cooled to room temperature with continued nitrogen flow. The catalyst samples were kept sealed in nitrogen until preparation for XPS.

2.2. Chemisorption experiments

The fresh catalysts were reduced in 5% H_2 in nitrogen at 170 °C for 1 h and then outgassed in nitrogen at 170 °C, as described previously [22]. Selected spent catalysts were outgassed in nitrogen at 170 °C before they were subjected to the same reduction treatment as the fresh catalysts. These catalysts were then subjected to CO adsorption measurements to determine the Pd surface area. Estimates of the Pd particle sizes were made from these CO adsorption measurements and are included in Table 1. The details of the

Table 1
Summary of previous results [22].

Catalyst: 5% Pd on	Support SA [m^2/g][a]	Catalyst SA [m^2/g][a]	CO adsorbed [μmol/g cat]	Pd SA [m^2/g][b]	Pd diameter [nm][c]	Yield [g/g cat][d]	Yield [g/g Pd][d]	TON[e]	Support NH_3 cm^3/g[f]	Support CO_2 cm^3/g[f]
n-Al_2O_3(+)	695	180	205	9.7	2	2.5	50	70	9.0	0.75
n-Al_2O_3(+) sp[g]	695	180	52	2.5	8.4	–	–	–	–	–
p-TiO_2	120	115	195	9.2	2	2.6	52	70	9.9	1.0
n-TiO_2	505	210	185	8.8	2.5	1.6	31	45	4.0	0.6
n-CeO_2	60	60	245	11.6	2	1.5	29	35	7.3	0.8
n-ZrO_2 (CeO_2)	45	40	145	6.9	3	2.45	49	110	2.6	1.1
n-ZrO_2	35	35	95	4.50	4.5	2.3	47	130	4.7	0.3
n-MgO	685	85	105	5.0	4	2.3	46	120	3.4	2.0
p-SiO_2	240	230	20	0.95	22	1.6	32	435	5.7	0.0
n-ZnO	70	35	75	3.6	6	2.1	44	150	14.3	0.2

[a] SA = surface area.
[b] Palladium surface area, calculated from the amount of CO adsorbed assuming a 1:1 Pd:CO ratio and a surface density of 1.42×10^{15} atoms/cm^2 [19].
[c] Pd particle size calculated from the Pd surface area.
[d] Yield of 4,4′-dimethyl-2,2′-bipyridine product per g catalyst or per g palladium.
[e] TON: turnover number, mol of product per mol surface palladium.
[f] Measured uptake of NH_3 (acidic sites) or CO_2 (basic sites) on the supports only (before palladium deposition).
[g] sp = spent, i.e. catalyst after reaction.

calculations for Pd dispersion, surface area and crystallite size are given in the previous work [22].

2.3. X-ray photoelectron spectroscopy

The fresh, spent and reduced catalyst powders were pressed into aluminum cups prior to insertion into the ultra-high vacuum (UHV) chamber (base pressure 1×10^{-10} Torr). XPS was performed using a double pass cylindrical mirror analyzer (PHI model 25-270 AR). Spectra were taken in retarding mode with a pass energy of 50 eV for survey spectra and 25 eV for high resolution spectra using a Mg Kα X-ray source (PHI 04-151). Data were collected using a computer interface and then digitally smoothed. A value for the C 1s binding energy of 284.6 eV was assigned to correct for static charging and work function differences [24].

The XPS spectra are presented without background subtraction. However, peak area analyses were carried out on spectra corrected using a Shirley background subtraction. In the case of the Pd 3d peaks from the ZrO_2-containing catalysts, this region was manually fitted with four Gaussian peaks: the Zr $3p_{3/2}$ and $3p_{1/2}$ and the Pd $3d_{5/2}$ and $3d_{3/2}$ peaks. The Pd 3d peak area was then calculated by integrating the two fitted Gaussian curves for the Pd $3d_{5/2}$ and $3d_{3/2}$ peaks. As the Gaussian peaks do not account for all the peak intensity in this region, the calculated peak areas for the Pd 3d peaks on the ZrO_2-containing catalysts are slightly underestimated. This does not significantly affect data interpretation as the trends in surface concentration between the ZrO_2 catalysts are investigated rather than actual concentrations.

For the Pd 3d, Zr 3d and Ti 2p peaks, both peaks, i.e. the $3d_{5/2}$ and $3d_{3/2}$ or $2p_{3/2}$ and $2p_{1/2}$, were integrated together since in all cases the peaks overlapped to some degree. The calculated peak areas were then corrected using the following atomic sensitivity factors; C 1s: 0.25, O 1s: 0.66, Pd 3d: 4.6, Ti 2p: 1.8, Zr 3d: 2.1 and Ce 3d: 10 [25] before the surface concentrations and peak-area ratios were calculated. As uncertainties are introduced using these atomic sensitivity factors, and since the catalyst compositions vary considerably in the near surface region, both laterally and vertically, only trends in concentrations and elemental ratios within a family of supports are discussed.

2.4. Transmission electron microscopy

TEM grids were prepared by dispersing the catalyst into water by ultrasonication and then placing a drop of the dispersion onto lacy carbon grids. After evaporation of the water, micrographs and energy dispersive spectroscopy (EDS) spectra were collected using a JEOL TEM 2010F instrument, with a 200 kV electron source. The PdO particles on the catalysts were identified using EDS at different spots on the catalysts, or by comparing the TEM pictures of bare supports to those of the respective catalysts.

2.5. X-ray diffraction

The XRD data were collected using a Philips powder X-ray diffractometer with a Bragg–Brentano geometry and Cu Kα radiation (λ = 1.54 Å). Diffraction patterns were obtained for selected calcined, reduced and spent catalysts. The catalyst powders were secured onto a glass slide with double-sided sticky tape. The average particle sizes were calculated from the line-broadening of the XRD peaks using the Scherrer equation

$$d = \frac{K\lambda}{\mathrm{FWHM}\ \cos(\theta)}$$

In this equation, K is a constant generally taken as unity, λ is the wavelength of the incident radiation, FWHM is the full width at half max and θ is the peak position.

3. Results and discussion

Results from previous studies are summarized in Table 1. The most active catalysts to date, with the highest product yield per gram of palladium, are PdO supported on n-Al_2O_3(+) or p-TiO_2, followed by PdO/n-ZrO_2(CeO_2), PdO/n-ZrO_2 and PdO/n-MgO. From Table 1 it is evident that there is no simple correlation between the catalytic activity and the Pd surface area or the support properties (surface area, acidity or basicity). Therefore, several catalysts were analyzed using XPS, TEM and XRD to obtain more information about the properties of importance for a high catalytic activity. As the proposed reaction mechanism is important for the discussion of these catalysts, it is presented in Fig. 1. It is our hypothesis that the pyridine nitrogen coordinates to the Pd^{2+} on the surface and the nearby oxygen of the PdO species facilitates the H abstraction. After two consecutive C–H insertions, a reductive elimination gives the bipyridine. Water is formed from the two hydroxyl groups on the surface, which also results in an oxygen vacancy. To close the catalytic cycle, oxygen must be added to the surface.

3.1. XPS analysis

All of the oxide-supported catalysts included in Table 1 were subjected to XPS measurements.

3.1.1. Titania-supported catalysts

Fresh PdO/p-TiO_2 and PdO/n-TiO_2 catalysts, as well as spent and reduced PdO/p-TiO_2 catalysts were analyzed using XPS to determine differences in surface composition and oxidation states between the two catalysts and between different treatments of the p-TiO_2-supported catalyst.

3.1.1.1. Fresh TiO_2 catalysts. The relative compositions and calculated elemental ratios from the TiO_2-supported palladium catalysts are given in Table 2. The main difference between the PdO/n-TiO_2 and PdO/p-TiO_2 catalysts appears to be that more Ti resides in the near surface region of the PdO/p-TiO_2 catalyst. Therefore, the Pd/Ti ratio is significantly higher for the PdO/n-TiO_2 catalyst. This difference is mainly due to the higher oxygen concentration on the PdO/n-TiO_2 catalyst and is likely caused by hydroxyl groups blocking the Ti at the surface (as indicated in the O 1s XPS peaks below).

As seen for the alumina-supported catalysts [26], the titania-supported catalyst with the broader Pd 3d peaks (PdO/p-TiO_2) exhibits the higher activity of the two PdO/TiO_2 catalysts (Fig. 2). The Pd $3d_{5/2}$ peaks are located at a slightly higher binding energy (336.3 eV) compared to the 336.1 eV value obtained from the PdO reference sample and the PdO/n-Al_2O_3(+) catalysts [26]. This

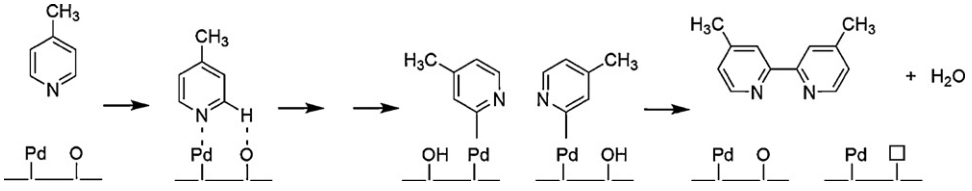

Fig. 1. Proposed reaction mechanism.

Table 2
Compositional results from XPS analysis.

Supports or 5% Pd catalysts										
TiO_2	C 1s	O 1s	Pd 3d	Ti 2p	Pd/Ti	Pd/C	Ti/C	Pd/O	Ti/O	C/O
p-TiO_2 support	24.2%	54.0%	–	21.7%	–	–	0.90	–	0.40	0.45
PdO/p-TiO_2 fresh	22.3%	54.8%	1.9%	21.0%	0.09	0.09	0.94	0.04	0.38	0.41
PdO/p-TiO_2 reduced	25.4%	53.0%	1.6%	20.0%	0.08	0.06	0.79	0.03	0.38	0.48
PdO/p-TiO_2 spent	24.0%	55.3%	0.9%	19.8%	0.05	0.04	0.82	0.02	0.36	0.43
PdO/p-TiO_2 spent sputtered	18.0%	57.8%	1.2%	23.0%	0.05	0.07	1.28	0.02	0.40	0.31
PdO/n-TiO_2 fresh	26.2%	59.9%	1.9%	12.0%	0.16	0.07	0.46	0.03	0.20	0.44

CeO_2	u‴/Ce 3d[a]	C 1s	O 1s	Pd 3d	Ce 3d	Pd/Ce	Pd/C	Ce/C	Pd/O	Ce/O	C/O
n-CeO_2 support	0.11	51.4%	28.9%	–	19.7%	–	–	0.38	–	0.68	1.78
PdO/n-CeO_2 fresh	0.08	54.5%	30.7%	3.1%	11.7%	0.26	0.06	0.21	0.10	0.38	1.77
PdO/n-CeO_2 reduced	0.07	48.4%	33.7%	2.7%	15.2%	0.18	0.06	0.31	0.08	0.45	1.44

ZrO_2	C 1s	O 1s	Pd 3d	Zr 3d	Pd/Zr	Pd/C	Zr/C	Pd/O	Zr/O	C/O
n-ZrO_2 support	22.0%	54.8%	–	23.2%	–	–	1.05	–	0.42	0.40
PdO/n-ZrO_2 fresh	23.9%	53.5%	3.6%	18.9%	0.19	0.15	0.79	0.07	0.35	0.45
PdO/n-ZrO_2 reduced	20.3%	55.3%	4.1%	20.3%	0.20	0.20	1.00	0.07	0.37	0.37
PdO/n-ZrO_2(CeO_2) fresh	21.1%	56.7%	4.4%	17.8%	0.25	0.21	0.84	0.08	0.31	0.37
PdO/n-ZrO_2(CeO_2) reduced	25.9%	52.4%	3.3%	18.4%	0.18	0.13	0.71	0.06	0.35	0.49
PdO/n-ZrO_2(CeO_2) spent	28.3%	50.6%	3.1%	18.0%	0.17	0.11	0.64	0.06	0.36	0.56

[a] Ratio of u‴ peak area over the total Ce 3d peak area (see Fig. 6).

reveals that the Pd^{2+} on the surface is more electron deficient compared to the Pd^{2+} in bulk PdO. While the n-TiO_2 also results in an electron deficient Pd^{2+} species on the surface, it is possible that the presence of hydroxyl groups already at the surface could hinder the H abstraction in the first step of the reaction mechanism (as active oxygen sites would be blocked by H before reaction, see Fig. 1). This in turn would explain why the n-TiO_2 is not as efficient a support as the p-TiO_2.

Unlike the Pd 3d peaks, there is no significant difference between the Ti 2p peaks obtained from the two catalysts (Fig. 3). However, palladium deposition appears to result in a small shift of the Ti $2p_{3/2}$ peak to a slightly lower binding energy (458.5 eV) relative to the bare support (458.6) for both the PdO/n-TiO_2 and PdO/p-TiO_2 catalysts. While this shift in the binding energies of the Ti $2p_{3/2}$ peaks is within the accuracy of the measurements, the shift in BEs of the Pd $3d_{5/2}$ peaks together with the results from the reduced and spent catalysts (*vide infra*) indicate that there are metal-support interactions on these catalysts. The transfer of electron density from palladium to titania is likely beneficial for the catalysts as it leads to a more electropositive palladium. An elec-

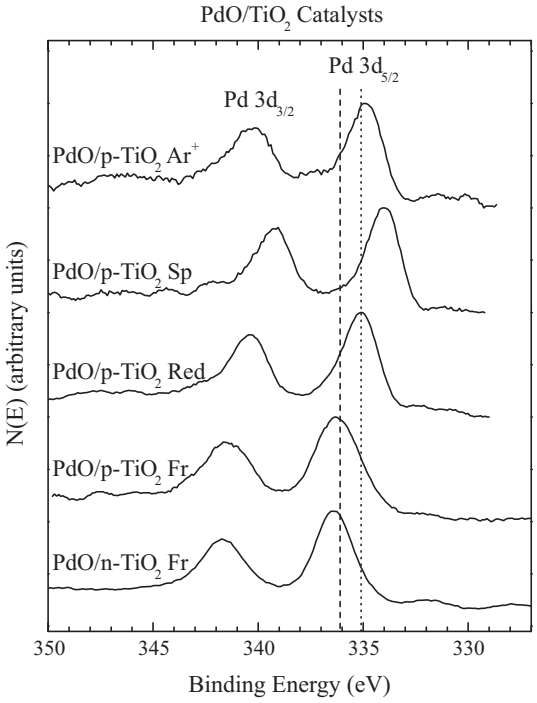

Fig. 2. Pd 3d peaks obtained from TiO_2-supported PdO catalysts. The dashed and dotted lines mark the Pd $3d_{5/2}$ peak positions of PdO and Pd metal, respectively. Fr: fresh; Red: reduced; Sp: spent; Ar^+: bombarded with argon ions.

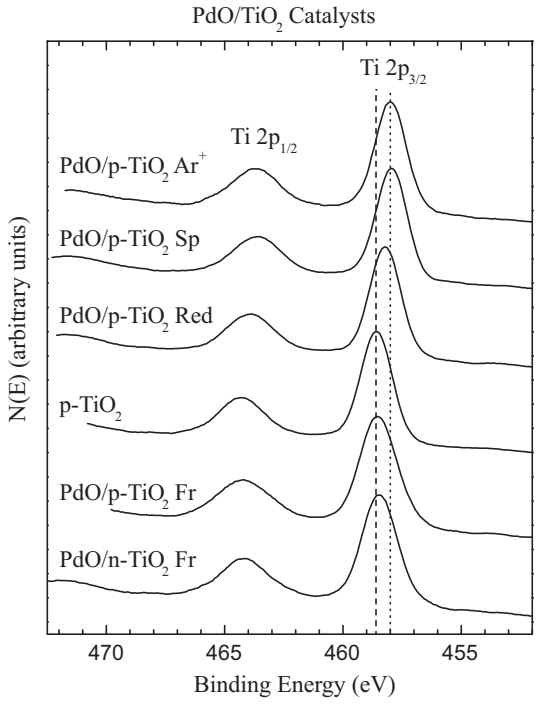

Fig. 3. Ti 2p peaks obtained from TiO_2-supported PdO catalysts. The dashed and dotted lines mark the Ti $2p_{3/2}$ peak positions of TiO_2 support and TiO_2-supported catalysts after reaction, respectively. Fr: fresh; Red: reduced; Sp: spent; Ar^+: bombarded with argon ions.

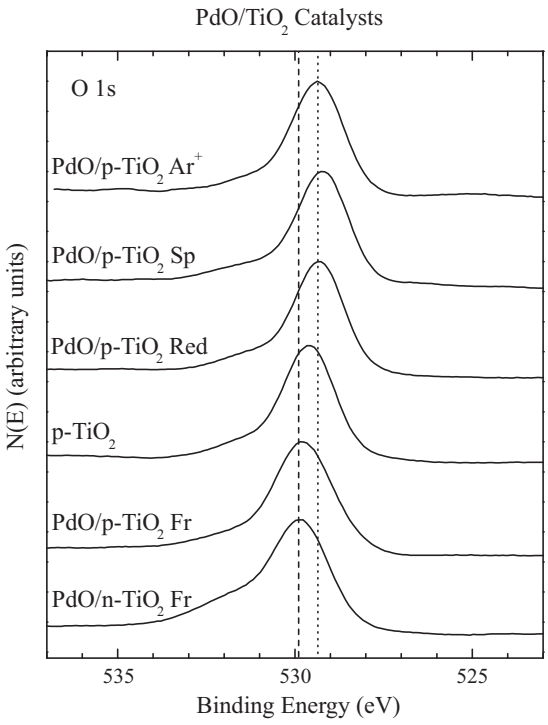

Fig. 4. O 1s peaks obtained from TiO_2-supported PdO catalysts. The dashed and dotted lines mark the O 1s peak positions of fresh catalysts and catalysts after reaction (or reduction), respectively. Fr: fresh; Red: reduced; Sp: spent; Ar^+: bombarded with argon ions.

tron deficient Pd^{2+} species can pull more electron density from the pyridine ring and results in a weakened C–H bond, which in turn facilitates the H abstraction step (Fig. 1).

The O 1s peaks obtained from the TiO_2-supported catalysts (Fig. 4) are shifted to slightly higher binding energies (529.8 eV) compared to that of the p-TiO_2 support (529.6 eV). This is most likely due to the contributions from PdO-related O 1s and Pd 3p peaks. Apart from the difference in Pd 3d peak width between the PdO/n-TiO_2 and PdO/p-TiO_2 catalysts, the only other significant difference in the XPS data from these catalysts is a higher oxygen concentration on the PdO/n-TiO_2 catalyst (Table 2). This higher oxygen concentration is due to a larger number of hydroxyl groups on the surface of the PdO/n-TiO_2 catalyst, which is evident as a shoulder at 531.7 eV on the O 1s peak in Fig. 4 (a $Ti(OH)_4$ or $TiO(OH)_2$ species increases the O:Ti ratio).

3.1.1.2. Reduced TiO_2 catalysts. Reduction of the PdO/p-TiO_2 catalyst in hydrogen at 170 °C reduces the PdO on the surface to Pd metal, as is evident in the lower binding energy of the Pd 3d peaks (335.1 eV) after the reductive treatment. However, there is still a shoulder at a binding energy of 336.3 eV. This shoulder likely indicates some surface oxidation after the reduction due to the brief air exposure during the sample transfer, although incomplete reduction of the PdO particles cannot be excluded. The reductive treatment also causes a shift of the O 1s peak from 529.8 to 529.3 eV and the Ti $2p_{3/2}$ peak shifts from 458.6 to 458.2 eV. The magnitude of the O 1s shift is higher than that expected from any changes in the PdO-related peaks during reduction of PdO to Pd metal. Similar shifts in the Ti $2p_{3/2}$ have been attributed to oxygen vacancies [27]. Consequently, this indicates that even mild reduction conditions induce oxygen vacancies on the porous TiO_2 support. This is not observed on the alumina support, but is in agreement with titania being classified as a reducible oxide and is an indication of strong metal-support interactions. Strong metal-support interactions are known to occur for catalysts consisting of precious metals supported on titania [28,29].

3.1.1.3. Spent TiO_2 catalysts. The amount of visible palladium is significantly lower and the carbon content higher on the spent PdO/p-TiO_2 catalyst compared to the fresh catalyst (Table 2). In contrast to the PdO/n-Al_2O_3(+) catalysts, for which the Pd/Al ratios were similar for the fresh and spent catalysts [26], the Pd/Ti ratio is significantly smaller on the spent PdO/p-TiO_2 compared with the fresh catalyst (Table 2). While the lower Pd/Ti ratio after reaction could be due to preferential deposition of carbon on Pd, the Pd/Ti ratio after Ar^+ sputtering indicates that this is not the case (*vide infra*).

The Pd $3d_{5/2}$ peak obtained from the spent PdO/p-TiO_2 catalyst has a very low binding energy, 334.0 eV (Fig. 2), which is below the 334.5 eV reported for high-dispersion surface Pd^0 [30]. This could be due to differential charging caused by carbon deposition. Therefore, the spent PdO/p-TiO_2 catalyst was sputtered to remove some of the surface carbon. After sputtering the carbon content on the catalyst is lower and the Pd $3d_{5/2}$ peak is located at 334.9 eV consistent with Pd metal [30] (Fig. 2). Removal of carbon increases the relative concentration of both Pd and Ti on the surface of the catalyst (Table 2) and does not alter the Pd/Ti ratio. Therefore, the Pd/Ti ratio is reduced during the reaction, indicating that either some palladium is leached into the reaction solution or that TiO_x species covers the palladium after reaction due to Pd or TiO_x migration. Any reduction in the Pd/Ti ratio is undesirable as it reduces the amount of active phase on the catalyst, and this negatively affects catalyst regeneration.

After reaction the Ti $2p_{3/2}$ peak is located at 458.0 eV, which is even lower than the Ti $2p_{3/2}$ binding energy of the reduced PdO/p-TiO_2 catalyst. It appears that there is efficient transfer of oxygen from the p-TiO_2 support to palladium, and this is likely the reason the PdO/p-TiO_2 is a highly active catalyst.

3.1.2. Ceria-supported catalysts

Fresh and reduced PdO/n-CeO_2 catalysts were also examined using XPS to probe metal-support interactions.

3.1.2.1. Fresh CeO_2 catalysts. The Pd 3d peaks obtained from the PdO/n-CeO_2 catalyst are located at very high binding energies (Fig. 5). The Pd $3d_{5/2}$ peak at 337.4 eV is higher than the binding energies reported for PdO in the NIST database (335.6–337.1 eV [31]). However, these high binding energies have been reported for CeO_2-supported, or CeO_2-promoted, palladium catalysts [32–34]. This together with the XPS data from the Ce 3d region indicate that the high binding energies are due to strong metal-support interactions rather than differential charging.

The Ce 3d peaks obtained from the nanoparticle CeO_2 are typical for a Ce^{4+} species (Fig. 6) [35]. The fine structure in this region is due to the empty Ce 4f orbitals, which give rise to two satellites each for the Ce $3d_{5/2}$ and Ce $3d_{3/2}$ peaks. This is in contrast to Ce^{3+}, which gives rise to a simpler spectrum with only one satellite for each of the Ce 3d peaks [35]. The extent of Ce^{4+} reduction to Ce^{3+} can be determined by calculating the ratio of the Ce^{4+}-specific $3d_{3/2}$ peak (u‴) area to the total Ce 3d peak area [32,36] (Fig. 6). The ratio for the nanoparticle CeO_2 is 0.11, which is slightly lower than the value reported in the literature for bulk CeO_2 (0.13) [37]. Deposition of palladium onto the CeO_2 support results in broadening of the Ce 3d peaks. The u‴ peak area ratio after palladium deposition is reduced to 0.08, which indicates reduction of some Ce^{4+} to Ce^{3+} species. This reveals strong metal support interactions that result in electron transfer from palladium to CeO_2, which gives an electron deficient Pd^{2+} species and is consistent with the high Pd 3d binding energies on this catalyst.

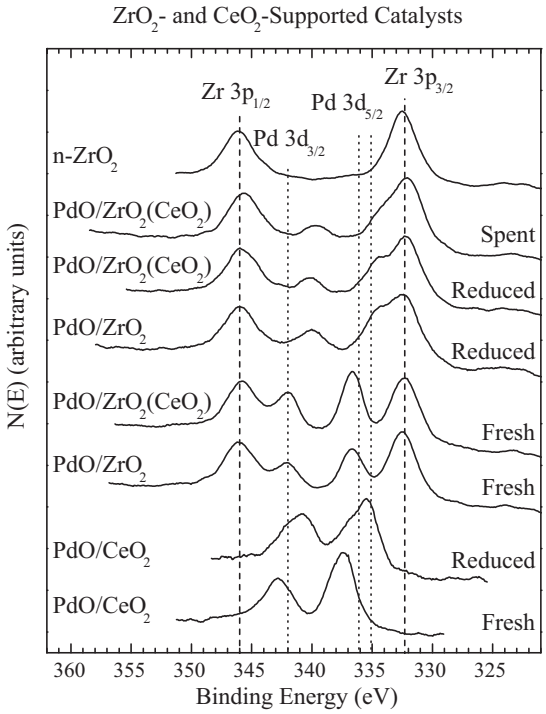

Fig. 5. Pd 3d peaks obtained from CeO_2- and ZrO_2-supported PdO catalysts. The dashed lines mark the peak positions of the Zr 3p peaks and the dotted lines indicate the positions of the Pd 3d peaks (PdO and Pd).

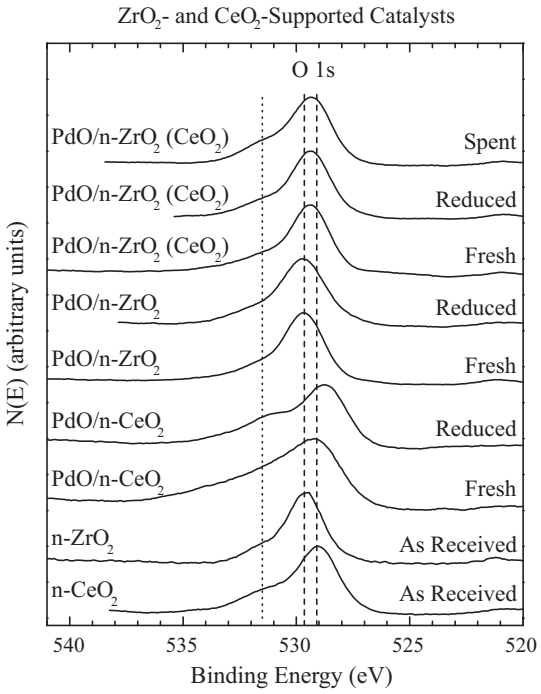

Fig. 7. O 1s peaks obtained from CeO_2- and ZrO_2-supported PdO catalysts. The dashed lines mark the O 1s peak positions of the n-ZrO_2 and n-CeO_2 supports. The dotted line indicates the O 1s peak position of OH-groups.

The O 1s peak obtained from the CeO_2 nanoparticles is located at 529.1 eV, in agreement with literature values (529.2 eV, Fig. 7) [31]. The O 1s peak obtained from the PdO/n-CeO_2 catalyst is significantly broader than that obtained from the CeO_2 support.

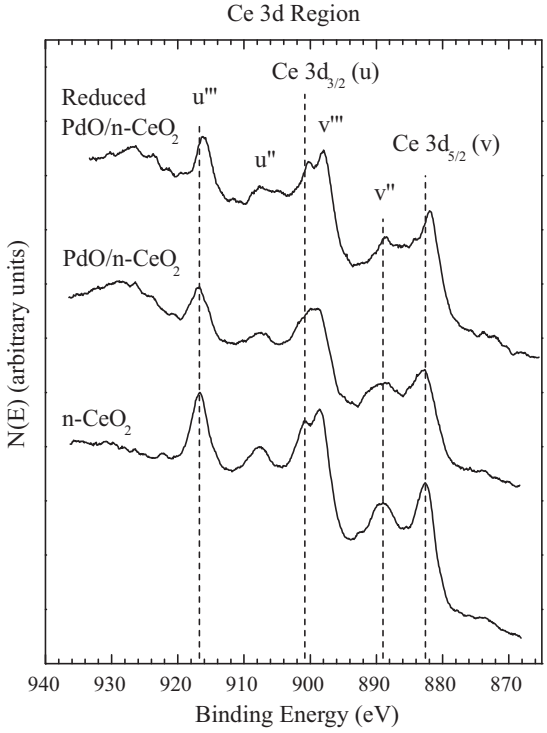

Fig. 6. Ce 3d peaks obtained from CeO_2-supported PdO catalysts. The dashed lines mark the peak positions of the Ce 3d peaks and some of the satellites obtained from the CeO_2 support.

Apparently there is a substantial contribution from species with binding energies of 534 eV and higher on this catalyst. This may be attributed to a high contribution from PdO_x; i.e. increased intensity at binding energies of 530.3 eV (O 1s of PdO) and above 533 eV (Pd $3p_{3/2}$ of PdO_x, where $x \geq 1$), and is consistent with both the high Pd $3d_{5/2}$ binding energy and the high Pd surface area relative to the total catalyst surface area (11.5 versus 60 m^2/g) on this catalyst. The presence of a large number of hydroxyl groups cannot be excluded either.

3.1.2.2. Reduced CeO_2 catalysts. Reductive treatment decreases the palladium content in the near surface region of the PdO/n-CeO_2 catalyst (Table 2). The carbon content is also reduced, while it is evident in Table 2 that more ceria is visible on the surface of this catalyst after reaction. The significantly lower Pd/Ce ratio after reduction could be due to migration of CeO_x that results in CeO_x-decoration of the palladium particles, which has been observed previously during low temperature reduction of PdO/CeO_2 [38,39].

The Pd 3d binding energies after exposure to reductive conditions reveal that the major species on the surface of the PdO/n-CeO_2 catalyst is Pd metal. However, there is a large shoulder at 336.6 eV in the spectrum obtained from this catalyst, which indicates that there is also a significant amount of oxidized palladium on the surface of this catalyst. The contribution from PdO is much higher on the reduced PdO/n-CeO_2 compared to reduced or spent PdO/p-TiO_2 and the PdO/n-Al_2O_3 catalysts in the previous study [26]. This is consistent with results from the literature, which have indicated that palladium on CeO_2 supports is easier to oxidize to PdO compared to palladium supported on other oxides [36]. Therefore, exposure to air at ambient conditions may be sufficient to cause oxidation of highly dispersed palladium on a ceria support. This again is indicative of strong metal-support interactions and could explain the high Pd dispersion and the reasonable activity of the PdO/n-CeO_2 catalyst despite the low initial support surface area. Unfortunately, in this case, the very strong metal-support interactions lead to migration of CeO_x over the palladium, which in turn reduces the

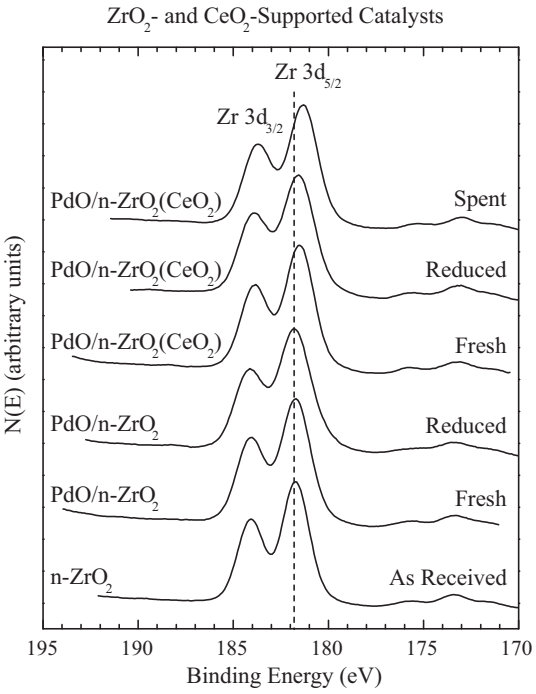

Fig. 8. Zr 3d peaks obtained from ZrO_2-supported PdO catalysts. The dashed line indicates the Zr $3d_{5/2}$ peak position of n-ZrO_2.

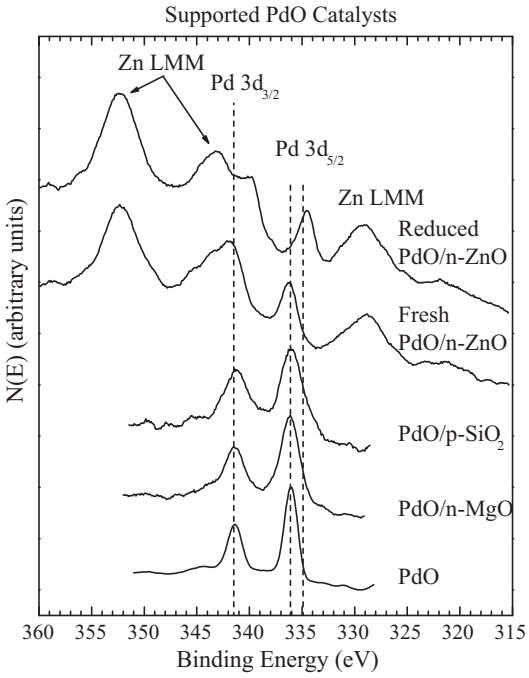

Fig. 9. Pd 3d peaks obtained from PdO supported on n-MgO, n-ZnO, and p-SiO_2. The dashed lines indicate the Pd 3d peak positions of PdO and Pd.

active sites and decreases the activity despite the favorable oxygen mobility properties. Furthermore, the presence of a high number of hydroxyl groups on the surface cannot be excluded, which could also hinder the reaction.

The Ce 3d peaks after reduction reveal a slight increase in the Ce^{3+} concentration (Ce_2O_3) compared to the fresh catalyst. The ratio of the Ce^{4+}-specific peak (u‴) area to the total Ce 3d peak area is reduced from 0.08 on the fresh catalyst to 0.07 on the reduced catalyst. This is in agreement with the Pd 3d data, where oxygen transfer from CeO_2 to Pd metal would result in more PdO compared to other supports with less mobile oxygen. The shift in the Ce 3d peaks to lower binding energies is another indication of strong metal support interactions.

3.1.3. Zirconia-supported catalysts

From Table 2 it is evident that the palladium signal intensities are higher on the PdO/n-ZrO_2(CeO_2) catalyst compared with the PdO/n-ZrO_2. This is in agreement with the higher dispersion on the PdO/n-ZrO_2(CeO_2) catalyst.

3.1.3.1. Fresh ZrO_2 catalysts. The Pd 3d region from the ZrO_2-containing catalysts is complicated by the Zr 3p peaks which overlap the Pd 3d peaks (Fig. 5). Quantification therefore requires resolution of the Pd and Zr peaks, as described in Section 2.3. Again, the higher Pd 3d to Zr 3p peak area ratio observed on the PdO/n-ZrO_2(CeO_2) catalyst compared with the non-doped PdO/n-ZrO_2 catalyst is evident in Fig. 5. The binding energies of the Pd $3d_{5/2}$ peaks are located at 336.6 eV for both the PdO/n-ZrO_2 and PdO/n-ZrO_2(CeO_2) catalysts. These Pd $3d_{5/2}$ binding energies are higher than those observed for the PdO/Al_2O_3 and PdO/TiO_2 catalysts (336.1–336.3 eV) indicating the presence of electron deficient Pd^{2+} species on the surface. This is likely due to strong palladium-support interactions.

Deposition of palladium onto the ZrO_2 supports results in slightly broader Zr 3d peaks (Fig. 8). There is an indication of a shoulder at low binding energies and the intensity in the region between the two Zr 3d peaks is increased. This suggests strong Pd–ZrO_2 interactions that lead to electron transfer from the Pd to ZrO_2. The Zr 3d peaks obtained from the CeO_2-doped nanoparticle ZrO_2 support are located at a slightly lower binding energy (181.5 eV) compared with the nanoparticle ZrO_2 support (181.8 eV, Fig. 8). This reveals strong electronic interactions also between the CeO_2 and the ZrO_2 in the support.

The O 1s binding energy region is naturally dominated by the oxygen atoms from the ZrO_2 support (Fig. 7). The O 1s peak obtained from the ZrO_2 nanoparticles is located at 529.7 eV. This binding energy is lower than the commonly reported 530.5 eV [31], but a value of 529.9 eV has been reported for ZrO_2 [40]. Adding 10% of CeO_2 to the ZrO_2 results in a significant shift in the O 1s peak to 529.4 eV which is in between the O 1s of ZrO_2 (529.7 eV) and CeO_2 (529.1 eV). This again indicates that the presence of CeO_2 significantly influences the ZrO_2 support.

3.1.3.2. Reduced ZrO_2 catalysts. In contrast to the PdO/n-CeO_2 catalyst, reduction of the PdO/n-ZrO_2 catalyst does not decrease the palladium content in the near surface region (see Table 2). Instead, removal of a significant amount of carbon during the reduction process results in a relative increase in palladium concentration in the near surface region. This is not true for the PdO/n-ZrO_2(CeO_2) catalyst, where the Pd/Zr ratio is lower after the reduction treatment. As for the PdO/n-CeO_2 catalyst, this is most likely due to migration of CeO_x over the palladium particles on the surface due to strong Pd–CeO_x interactions. Evidently, the ZrO_2 is less prone to reduction and migration over the Pd particles revealing that Pd–ZrO_2 interactions may be weaker compared to Pd–CeO_2 interactions. The latter is supported by the higher Pd $3d_{5/2}$ binding energy on the CeO_2 support versus the ZrO_2 support. This is also evidenced by the lower contribution from PdO on the surface of reduced PdO/n-ZrO_2 compared with the reduced PdO/n-CeO_2 catalyst (Fig. 5). However, due to the overlapping Zr 3p peaks in this region, quantifying the contribution from PdO on the reduced PdO/n-ZrO_2 catalysts is difficult.

For both the PdO/n-ZrO_2 and PdO/n-ZrO_2(CeO_2) catalysts, reduction alters the Zr 3d peaks slightly. A small shoulder at low binding energies appears on both reduced catalysts. This may be due to the introduction of some oxygen vacancies (ZrO_{2-x}) after the

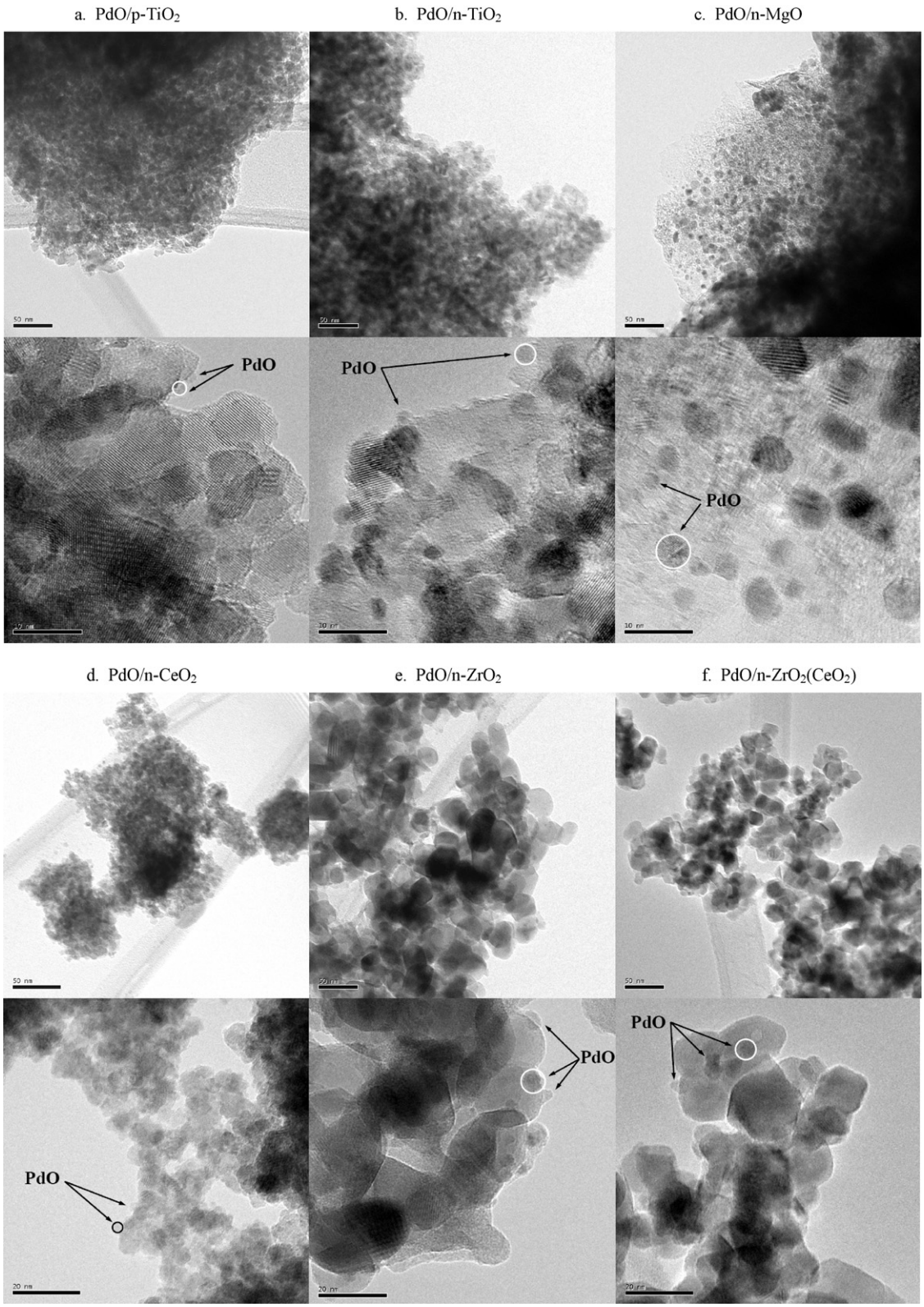

Fig. 10. TEM pictures obtained from (a) PdO/p-TiO_2, (b) PdO/n-TiO_2, (c) PdO/n-MgO, (d) PdO/n-CeO_2, (e) PdO/n-ZrO_2, and (f) PdO/n-$ZrO_2(CeO_2)$ catalysts. The scale bars are 50 nm for the top figures, and 10 nm (a–c) or 20 nm (d–f) for the bottom figures.

reductive treatment and is in agreement with ZrO_2 being classified as an interacting support [41].

3.1.3.3. Spent $ZrO_2(CeO_2)$ catalyst. The spent PdO/n-$ZrO_2(CeO_2)$ catalyst is reduced with Pd metal being the major palladium species on the surface (Fig. 5), and more carbon is present on the surface after exposure to the reaction conditions (Table 2). The Pd/Zr ratio is significantly reduced after reaction, which may partly be due to CeO_x migration onto the palladium because this would increase the Zr and decrease the Pd content in the near surface region. How-

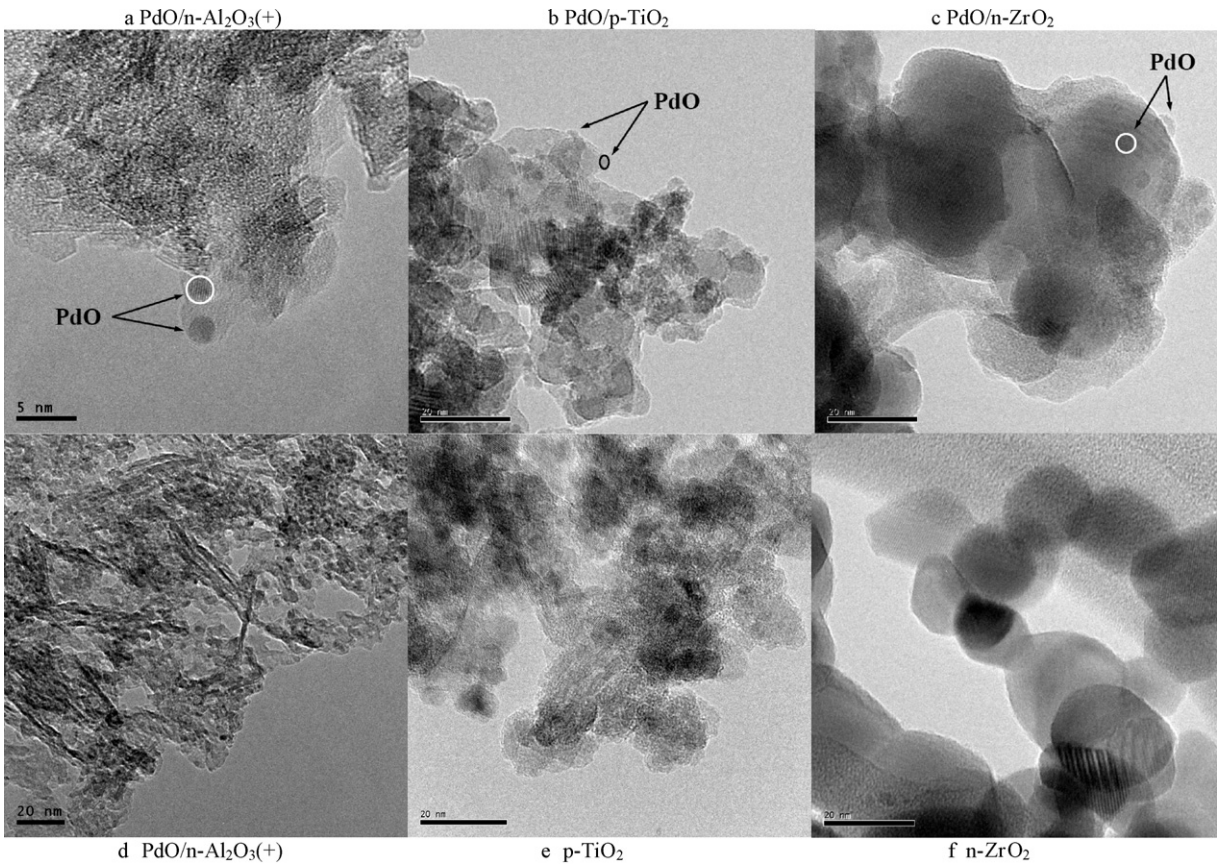

Fig. 11. TEM pictures obtained from (a) PdO/n-Al_2O_3(+), (b) PdO/p-TiO_2, (c) PdO/n-ZrO_2, (d) PdO/n-Al_2O_3(+), (e) p-TiO_2, (f) n-ZrO_2. The scale bars are 20 nm for all figures, except for the high-resolution image of the PdO/n-Al_2O_3(+) catalyst figure (a), where the scale bar is 5 nm.

ever, the Pd/Zr ratio is slightly lower on the spent catalyst compared with the reduced PdO/n-ZrO_2(CeO_2) catalyst, which could indicate that some palladium is lost from the surface of this catalyst due to leaching into the reaction solution or that carbon is preferentially deposited on the palladium.

3.1.4. Metal-oxide-supported catalysts

For comparison, three additional catalysts were characterized with XPS; PdO/n-MgO, PdO/p-SiO_2 and PdO/n-ZnO. They were selected to determine if the previous classification of interacting/non-interacting supports could be confirmed [22].

3.1.4.1. Fresh catalysts. The Pd 3d peaks obtained from the fresh PdO/n-MgO, PdO/p-SiO_2 and PdO/n-ZnO catalysts are presented in Fig. 9. The Pd $3d_{5/2}$ binding energies of the palladium supported on n-MgO and p-SiO_2 are consistent with those of PdO/Al_2O_3 [26] and bulk PdO (336.1 eV). In contrast, the Pd $3d_{5/2}$ peak obtained from fresh PdO/n-ZnO is located at 336.3 eV, which is similar to the Pd $3d_{5/2}$ binding energy obtained from PdO/TiO_2 but lower than those obtained from PdO/n-CeO_2 (337.4 eV) and PdO/ZrO_2 (336.6 eV) catalysts. These binding energies are consistent with the previous conclusion that n-MgO, p-SiO_2 and Al_2O_3 [all the alumina supports tested; γ-Al_2O_3, n-Al_2O_3(−) and n-Al_2O_3(+)] are non-interacting supports; i.e. they do not induce strong electronic metal-support interactions, while n-ZnO, p-TiO_2, n-CeO_2, and n-ZrO_2 result in medium to strong metal-support interactions. The only exception of the catalysts investigated is PdO/n-TiO_2, which behaves like a catalyst on a non-interacting support even though the Pd $3d_{5/2}$ binding energy is 336.3 eV. In the case of TiO_2, this could be due to the presence of hydroxyl groups on the fresh catalysts, and the crystal structure of the support is also important (see Section 3.3.1.1).

The XPS results also support the observation that strong metal-support interactions can result in high palladium dispersions relative to the support surface area and higher than expected catalytic activities from the measured Pd surface area. However, the catalytic activities do not exhibit a simple correlation with either palladium surface area or metal-support interaction strength. This may indicate that the reaction is structure sensitive and only PdO particles of certain size or structure are active in the reaction.

3.2. TEM/EDS data

Selected catalysts were subjected to TEM measurements. Representative micrographs obtained from PdO/p-TiO_2, PdO/n-TiO_2, PdO/n-MgO, PdO/n-CeO_2, PdO/n-ZrO_2, and PdO/n-ZrO_2(CeO_2) are presented in Fig. 10. For comparison, the data obtained from PdO/n-Al_2O_3(+) is included in Fig. 11. The PdO particles are visible as small darker spots (see arrows and circles in Fig. 10) and the particle sizes observed in the TEM micrographs are reasonably consistent with those expected from the Pd particle sizes calculated using the CO adsorption measurements. Identifying the PdO particles on the support is facilitated by comparing TEM images obtained from the bare supports and the catalysts. Representative micrographs from p-TiO_2 and n-ZrO_2 catalysts and supports are included in Fig. 11. In the case of the n-Al_2O_3(+)-supported catalyst, the crystalline PdO particles are easily identified on the nearly amorphous alumina support (Fig. 11a).

Compared to the PdO/n-Al_2O_3(+) studied in the previous work, the catalysts in the present study are composed of supports which exhibit less fine structure; i.e. no nanometer sized rods or strands (Figs. 10 and 11). However, the p-TiO_2, n-TiO_2 and n-CeO_2 reveal small (10 nm or less) support particles in the agglomerates (Fig. 10, top images). The particle sizes of the n-ZrO_2 and n-ZrO_2(CeO_2)

are larger, but consistent with the 20–30 nm oxide particle size reported from the vendor. The larger support particle sizes for the n-ZrO_2 and n-ZrO_2(CeO_2) supports (Fig. 10e and f) relative to the n-CeO_2 support (Fig. 10d) are expected considering the lower surface areas of the n-ZrO_2-based supports (Table 1). The smaller support particle size of the n-ZrO_2(CeO_2) relative to the n-ZrO_2 support is also consistent with the slightly higher surface area measured on the n-ZrO_2(CeO_2) support. The support particle size of the PdO/n-MgO catalyst is more difficult to discern in Fig. 10c. Compared to the other catalysts, the PdO/n-MgO appears to be more agglomerated. This is consistent with the significant smaller surface area of the catalyst (85 m^2/g) compared to the support (685 m^2/g, Table 1). The PdO/n-MgO surface area is significantly smaller than that of PdO/n-Al_2O_3(+) (180 m^2/g), which is a support with similar surface area to the n-MgO.

The main differences between the PdO/p-TiO_2 and PdO/n-TiO_2 catalysts appear to be (1) a more crystalline TiO_2 structure for the PdO/p-TiO_2 catalyst and (2) a less uniform distribution of PdO particle sizes for the PdO/n-TiO_2 catalyst. This is consistent with the XRD data obtained from these catalysts and the slightly lower Pd surface area measured on the PdO/n-TiO_2 catalyst. A stronger Pd–TiO_2 interaction on the anatase phase is consistent with the higher dispersion, and the more crystalline structure of the PdO/p-TiO_2 catalyst compared with the PdO/n-TiO_2 catalyst.

The PdO/n-CeO_2 catalyst exhibits very fine structure, and the visible small PdO particles appear to be consistent with both the high Pd dispersion and the Pd particle sizes reported for the reduced catalyst. The small PdO particles are easily identified on the PdO/n-ZrO_2 catalyst when comparing the TEM obtained from the catalyst to the one obtained from the bare n-ZrO_2 support (Fig. 11c and f). The PdO particle sizes on the ZrO_2-supported catalysts are reasonably consistent with the Pd particle sizes (3–4.5 nm) calculated from the Pd surface area measurements. This suggests that the reductive treatment before the CO chemisorption measurements does not result in significant sintering of the palladium on the support.

3.3. XRD data analysis

As it is difficult to detect small PdO particles on highly crystalline supports, only selected catalysts were subjected to XRD analysis.

3.3.1. Titania-supported catalysts

The titania supports and selected TiO_2-supported catalysts were analyzed using XRD to determine the crystal structure of the supports and if the palladium species can be detected using this technique.

3.3.1.1. Fresh TiO_2 catalysts. The XRD patterns obtained from the n-TiO_2 and p-TiO_2 supports as well as the PdO/p-TiO_2 catalysts are presented in Fig. 12. The n-TiO_2 support has poor crystallinity. An anatase phase can be discerned [42], but at least one other crystalline phase is present. In agreement with the TEM data, the p-TiO_2 is much more crystalline, and the anatase is the only detectable phase in this support. As the anatase TiO_2 phase has been shown to result in stronger palladium-support interactions compared to other TiO_2 phases (such as rutile) [43], the TiO_2 phase may explain the observed differences in the properties of the PdO/p-TiO_2 and PdO/n-TiO_2 catalysts. The anatase phase present in the PdO/p-TiO_2 catalyst, with its stronger Pd–TiO_2 interactions, may explain why the p-TiO_2 support with a surface area of 120 m^2/g results in a catalyst with a higher palladium dispersion compared with the n-TiO_2 support with a surface area of 505 m^2/g. The PdO/p-TiO_2 catalyst also has a higher turnover number than the PdO/n-TiO_2, indicating more favorable palladium-support interactions, which result in more active palladium species. This is consistent with the previous classification of p-TiO_2 as an interacting oxide inducing palladium-support interactions, while n-TiO_2 behaves as a non-interacting oxide [22].

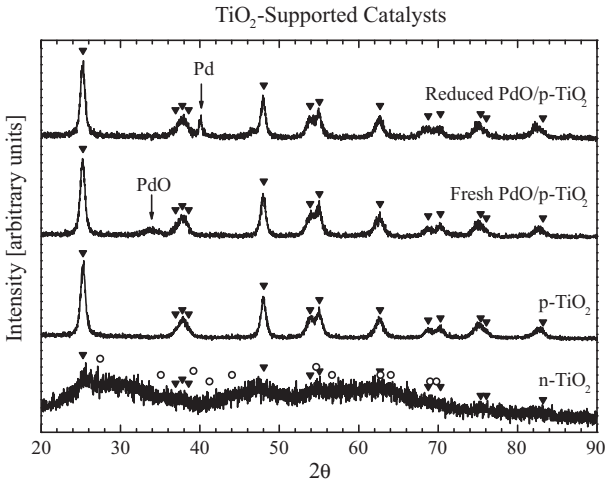

Fig. 12. XRD patterns obtained from TiO_2 supports and TiO_2-supported PdO catalysts. Peak positions for anatase TiO_2 (▼) and rutile TiO_2 (○) are indicated.

The PdO particle size of the fresh PdO/p-TiO_2 catalyst calculated from the Scherrer equation and the line broadening of the peak (full width at half maximum after peak deconvolution) is ~4.0 nm. This PdO particle size is larger than that observed on the PdO/n-Al_2O_3 catalyst (2.9 nm), but it is consistent with the slightly higher Pd surface area measured on the PdO/n-Al_2O_3 catalyst, particularly considering the uncertainties associated with particle size estimation using XRD.

3.3.1.2. Spent and reduced TiO_2 catalysts. A spent PdO/p-TiO_2 catalyst was also subjected to XRD analysis to determine if only the near surface region is reduced during the reaction. The region between $2\theta = 30^\circ$ and 45° is presented in Fig. 13a. As was the case for the n-Al_2O_3(+)-supported catalysts [26], no PdO can be detected in the spent catalyst. In fact, experiments reveal that the reduction of PdO on the surface is fast relative to the time of reaction (72 h). XRD analysis on a catalyst removed after only an hour of reaction does not detect any PdO in the catalyst, and the XRD spectrum (not shown) is very similar to the one obtained from the spent catalyst after 72 h of reaction. While the presence of amorphous PdO, or a very small PdO core of the particles, cannot be excluded, this indicates that the crystalline PdO in this catalyst is fully reduced during reaction, i.e. not only the surface but also most of the bulk PdO. This is an important observation since complete reduction of PdO to Pd metal on the catalyst surface likely results in a species that is much more difficult to reoxidize than a PdO particle with a Pd surface layer. *It also suggests that a surface oxide is the active species during reaction*. The Pd particle size on the spent catalyst is estimated to be slightly larger than the PdO particle size on the fresh catalyst; 4.6 versus 4.0 nm, respectively. This could be due to some particle growth during reaction or preferential leaching of the smaller particle sizes. However, considering the uncertainties in the particle size estimation from a fitted XRD peak width and the Scherrer equation, the difference in particle size is not significant. For comparison, the Pd particle size obtained from a catalyst exposed to reductive treatment is 5.1 nm. This is considerably larger than the particle size calculated based on the measured Pd surface areas (2.4 nm) and indicates the presence of amorphous palladium phases or very small (below 1–2 nm diameter) palladium particles that cannot be detected with XRD.

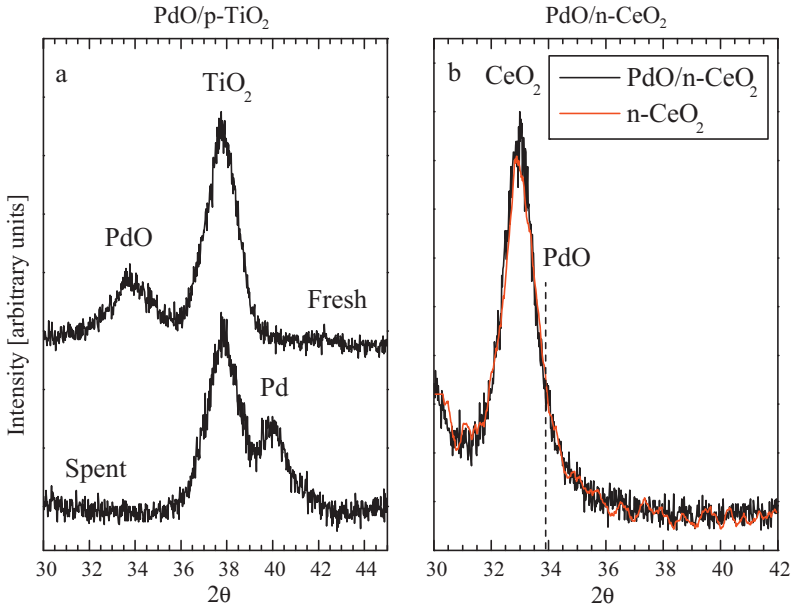

Fig. 13. High-resolution XRD patterns obtained from (a) TiO_2- and (b) CeO_2-supported PdO catalysts.

3.3.2. Ceria-supported catalysts

The XRD spectra obtained from n-CeO_2 and the fresh PdO/n-CeO_2 catalyst are presented in Fig. 14. The cubic phase of ceria is evident in these samples [44]. The catalyst preparation procedure does not alter the support structure or particle size significantly. No peaks due to PdO are apparent in the spectrum obtained from the fresh PdO/n-CeO_2 catalyst. While this may be partly due to the overlap of the main PdO peaks, (1 0 1) and (0 0 2) [45], with the (2 0 0) peak of the CeO_2 support (Fig. 14) [44], no other peak due to PdO can be resolved nor is there a measurable shoulder on the CeO_2 (2 0 0) peak due to the main PdO peaks in the high-resolution spectra obtained from this catalyst (Fig. 13b). The PdO on the surface of this support probably is amorphous and thus XRD invisible or the particle sizes could be below the XRD detection limit, which would be consistent with the higher CO uptake and larger calculated Pd surface area compared with the PdO/n-Al_2O_3(+) catalyst. However, a complicating factor for the CeO_2 support is that the scattering factor of cerium is much higher relative to palladium compared to the differences between palladium and titanium or palladium and aluminum. This results in a significantly higher contribution from the oxide support to the XRD signal obtained from the PdO/n-CeO_2 compared to the PdO/n-Al_2O_3(+) and PdO/p-TiO_2 catalysts. Consequently, the PdO signal may be obfuscated in the ceria background on the PdO/n-CeO_2 catalyst.

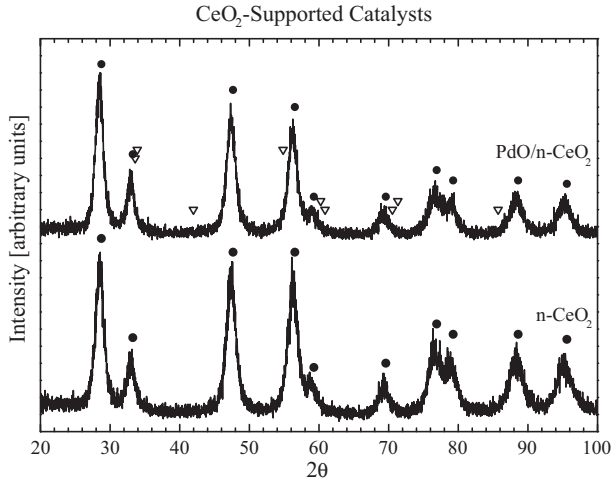

Fig. 14. XRD patterns obtained from n-CeO_2 and PdO/n-CeO_2. Peak positions for cubic CeO_2 (●) and tetragonal PdO (▽) are indicated.

4. Conclusions

The catalyst characterizations in this study have provided a significant amount of information about the behavior of palladium supported on various oxides.

The XPS analysis of the Pd $3d_{5/2}$ binding energy (BE) region confirms our previous hypothesis of interacting and non-interacting supports. The PdO on the non-interacting supports (n-Al_2O_3(+), n-MgO and p-SiO_2), in all cases have Pd $3d_{5/2}$ BEs of 336.1 eV, which is consistent with bulk PdO. The oxides classified as interacting supports; p-TiO_2, n-ZnO, n-ZrO_2, n-ZrO_2(CeO_2), and n-CeO_2, all have electron deficient Pd^{2+} species on the surface, i.e. Pd $3d_{5/2}$ BEs ranging from 336.3 to 337.4 eV. Metal-support interactions leading to electron deficient palladium species are likely beneficial to the reaction, as the palladium will pull electrons from the pyridine nitrogen and thereby weaken the nearby C–H bonds, which in turn could facilitate the subsequent H abstraction. Strong metal-support interactions on reducible supports or supports with mobile oxygen are likely also advantageous as they could lead to oxygen transfer from the support to the palladium and thus regenerate the active PdO species on the surface. Another benefit of strong metal-support interactions is that it can lead to high palladium surface areas on the catalysts. This is indeed observed on the PdO/n-CeO_2, PdO/n-ZrO_2(CeO_2) and PdO/n-ZrO_2 catalysts, as the palladium dispersions on these catalysts are significantly higher than expected from the support surface areas (35–60 m^2/g).

The Pd $3d_{5/2}$ BE of 336.3 eV on the PdO/n-TiO_2 catalyst is consistent with an interacting support, and explains the high Pd surface area measured on this catalyst. However, the XPS data also reveals that there is a significant amount of hydroxyl groups on the PdO/n-TiO_2 catalyst, which could hinder the reaction. Another important observation that may explain the difference in catalytic behavior between the PdO/p-TiO_2 and PdO/n-TiO_2 catalyst is that the p-TiO_2 support consists of a crystalline anatase phase, while the n-TiO_2 is

mainly amorphous. As an anatase phase is expected to result in favorable Pd–TiO_2 interactions, this is a significant difference.

The XPS data also indicates that there is likely an optimum Pd-support interaction. If the Pd-support interactions are too strong, as in the case of the n-CeO_2 support, it can lead to migration of support species over the palladium. This in turn reduces the active metal surface area and results in a decreased catalytic activity and a lower than expected turnover number.

XRD analysis reveals that all the PdO on the surface of the PdO/p-TiO_2 catalyst reduces very quickly. This indicates that a surface oxide is likely the active species and reveals that reoxidation is a critical step in the reaction.

In summary, metal-support interactions leading to an electron-deficient palladium species on the surface is beneficial for the reaction as long as the migration of the promoter over the palladium and palladium leaching into the solution during reaction can be suppressed. It is possible that the catalytic activity of these catalysts can be improved by adding promoters with mobile oxygen to high surface area supports.

Acknowledgments

Acknowledgment is made to the donors of the American Chemical Society Petroleum Research Fund for support of this research.

XRD measurements were performed at the Major Analytical Instrumentation Center at the University of Florida. The authors are thankful for the advice and instruction of Dr. Valentin Craciun. The authors also wish to thank Drs. Amelia Dempere, Kerry Siebein and Gerald Bourne at MAIC for assistance with collecting and interpreting the TEM images.

Justin Dodson is gratefully acknowledged for his assistance with this manuscript.

References

[1] A.K. Santra, D.W. Goodman, Electrochim. Acta 47 (2002) 3595.
[2] S.-H. Oh, G.B. Hoflund, J. Catal. 245 (2007) 35.
[3] P. Gélin, M. Primet, Appl. Catal. B 39 (2002) 1.
[4] T.V. Choudhary, S. Banerjee, V.R. Choudhary, Appl. Catal. A 234 (2002) 1.
[5] D. Ciuparu, M.R. Lyubovsky, E. Altman, L.D. Pfefferle, A. Datye, Catal. Rev. Sci. Eng. 44 (2002) 593.
[6] M. Hosseini, S. Siffert, H.L. Tidahy, R. Cousin, J.-F. Lamonier, A. Aboukais, A. Vantomme, M. Roussel, B.-L. Su, Catal. Today 122 (2007) 391.
[7] P. Papaefthimiou, T. Ioannides, X.E. Verykios, Appl. Catal. B 13 (1997) 175.
[8] E.M. Cordi, J.L. Falconer, J. Catal. 162 (1996) 104.
[9] D. Ciuparu, A. Ensuque, F. Bozon-Verduraz, Appl. Catal. A 326 (2007) 130.
[10] M. Besson, P. Gallezot, Catal. Today 57 (2000) 127.
[11] J. Tsuji, Palladium Reagents and Catalysis: Innovation in Organic Synthesis, Wiley, Chichester, UK, 1995.
[12] J.-L. Malleron, J.-C. Fiaud, J.-Y. Legros, Handbook of Palladium-Catalyzed Organic Reactions, Academic Press Limited, London, UK, 1997.
[13] G. Dyker, Angew. Chem. Int. Ed. 38 (1999) 1698.
[14] G.D.F. Jackson, W.H.F. Sasse, C.P. Whittle, Aust. J. Chem. 16 (1963) 1126.
[15] P.E. Rosevear, W.H. Sasse, Patent App. No. 40930/72, 1973, p. 1.
[16] S. Munavalli, M. Gratzel, Chem. Ind. (1987) 722.
[17] GFS Chemicals http://www.gfschemicals.com/statics/productdetails/DIMETHYL_BIPYRIDINE_127.html (accessed 06.21.10).
[18] P.E. Rosevear, W.H.F. Sasse, J. Heterocycl. Chem. 8 (1971) 483.
[19] L.M. Neal, H. Hagelin-Weaver, J. Mol. Catal. A 284 (2008) 141.
[20] n-Al_2O_3(+): NanoScale NanoActive Alumina Plus, http://www.nanoscalecorp.com/content.php/chemicals/powders/. Properties: $\geq$550 m^2/g.
[21] Alfa Aesar TiO_2 catalyst support. Properties: anatase with surface area 150 m^2/g.
[22] L.M. Neal, H. Hagelin Weaver, J. Mol. Catal. A 307 (2009) 29.
[23] The n-Al_2O_3(+), n-CeO_2, n-MgO, n-ZnO, n-TiO_2 were obtained from NanoScale Corporation (http://www.nanoscalecorp.com/content.php/chemicals/powders/), the n-ZrO_2 and n-ZrO_2(CeO_2) were obtained from Nanostructured & Amorphous Materials Inc. (http://www.nanoamor.com/nanoscale_elements_oxides__carbides___nitrides) and the p-SiO_2 and p-TiO_2 were obtained from Alfa Aesar (http://www.alfa.com/en/gh100w.pgm) (accessed on 09.15.10).
[24] C.D. Wagner, W.M. Riggs, L.E. Davis, J.F. Moulder, G.E. Muilenberg (Eds.), Handbook of X-ray Photoelectron Spectroscopy, Perkin-Elmer Corp.: Eden Prairie, MN, 1979.
[25] Atomic sensitivity factors taken from the following web page: http://www.uksaf.org/data/sfactors.html (accessed 06.14.10: C.D. Wagner, L.E. Davis, M.V. Zeller, J.A. Taylor, R.M. Raymond, L.H. Gale, Surf. Interface Anal. 3 (1981) 211).
[26] L.M. Neal, S.D. Jones, M.L. Everett, G.B. Hoflund, H.E. Hagelin-Weaver, J. Mol. Catal. A 325 (2010) 25.
[27] G. Tian, L. Dong, C. Wei, J. Huang, H. He, J. Shao, Opt. Mater. 28 (2006) 1058.
[28] See for example A.K. Datye, D.S. Kalakkad, M.H. Yao, D.J. Smith, J. Catal. 155 (1995) 148, and references therein.
[29] G.B. Hoflund, A.L. Grogan Jr., D.A. Asbury, J. Catal. 109 (1988) 226.
[30] C.E. Gigola, M.S. Moreno, I. Costilla, M.D. Sanchez, Appl. Surf. Sci. 254 (2007) 325.
[31] National Institute of Standards and Technology, NIST on-Line XPS Database http://srdata.nist.gov/xps/intro.aspx (accessed 06.14.10).
[32] J.Z. Shyu, K. Otto, W.L.H. Watkins, G.W. Graham, R.K. Belitz, H.S. Gandhi, J. Catal. 114 (1988) 23.
[33] A.L. Guimaraes, D.C. Dieguez, M. Schmal, An. Acad. Braz. Cienc 76 (2004) 825.
[34] J.M. Padilla, G. Del Angel, J. Navarrete, Catal. Today 133–135 (2008) 541.
[35] D.R. Mullins, S.H. Overbury, D.R. Huntley, Surf. Sci. 409 (1998) 307.
[36] P.A. Weyrich, H. Treviño, W.F. Hölderich, W.M.H. Sachtler, Appl. Catal. A 163 (1997) 31.
[37] J.Z. Shyu, W.H. Weber, H.S. Gandhi, J. Phys. Chem. 92 (1988) 4964.
[38] A. Badri, C. Binet, J.C. Lavalley, J. Chem. Soc., Faraday Trans. 92 (1996) 1603.
[39] S. Naito, T. Kasahara, T. Miyao, Catal. Today 74 (2002) 201.
[40] D.D. Sarma, C.N.R. Rao, J. Electron Spectrosc. Relat. Phenom. 20 (1980) 25.
[41] S. Ahmed Jalal, D.-J. Zhang, M. Machida, Catal. Commun. 10 (2008) 192.
[42] Anatase JCPDS International Center for Diffraction Data #22-1272, 1996, [ref database].
[43] Y. Li, Y. Fan, H. Yang, B. Xu, L. Feng, M. Yang, Y. Chen, Chem. Phys. Lett. 372 (2003) 160.
[44] JCPDS International Center for Diffraction Data #43-1002, 1996, [ref. database].
[45] JCPDS International Center for Diffraction Data #6-515, 1996, [ref. database].